BIOCHEMISTRY
including biophysical chemistry & molecular biology

Article

pubs.acs.org/biochemistry

Three-Dimensional Structure and Interaction Studies of Hepatitis C Virus p7 in 1,2-Dihexanoyl-*sn*-glycero-3-phosphocholine by Solution Nuclear Magnetic Resonance

Gabriel A. Cook, Lindsay A. Dawson, Ye Tian, and Stanley J. Opella*

Department of Chemistry and Biochemistry, University of California at San Diego, La Jolla, California 92093, United States

ABSTRACT: Hepatitis C virus (HCV) protein p7 plays an important role in the assembly and release of mature virus particles. This small 63-residue membrane protein has been shown to induce channel activity, which may contribute to its functions. p7 is highly conserved throughout the entire range of HCV genotypes, which contributes to making p7 a potential target for antiviral drugs. The secondary structure of p7 from the J4 genotype and the tilt angles of the helices within bilayers have been previously characterized by nuclear magnetic resonance (NMR). Here we describe the three-dimensional structure of p7 in short chain phospholipid (1,2-dihexanoyl-*sn*-glycero-3-phosphocholine) micelles, which provide a reasonably effective membrane-mimicking environment that is compatible with solution NMR experiments. Using a combination of chemical shifts, residual dipolar couplings, and PREs, we determined the structure of p7 using an implicit membrane potential combining both CS-Rosetta decoys and Xplor-NIH refinement. The final set of structures has a backbone root-mean-square deviation of 2.18 Å. Molecular dynamics simulations in NAMD indicate that several side chain interactions might be taking place and that these could affect the dynamics of the protein. In addition to probing the dynamics of p7, we evaluated several drug−protein and protein−protein interactions. Established channel-blocking compounds such as amantadine, hexamethylene amiloride, and long alkyl chain iminosugar derivatives inhibit the ion channel activity of p7. It has also been shown that the protein interacts with HCV nonstructural protein 2 at the endoplasmic reticulum and that this interaction may be important for the infectivity of the virus. Changes in the chemical shift frequencies of solution NMR spectra identify the residues taking part in these interactions.

Hepatitis C virus (HCV) chronically infects more than 150 million people and causes more than 350000 deaths per year (World Health Organization, 2012). It is a member of the *Hepacivirus* genus within the Flaviviridae family.[1] Currently, no vaccines exist for HCV, and the treatment regime of interferon-α and ribavirin is poorly tolerated, costly, and only effective in approximately 50% of patients. Recent trials of drugs that inhibit viral enzymes have been disappointing because of the rapid development of resistance by the virus.[2−4] Because of the high variability in HCV genotypes, new treatments in all likelihood will require combinations of drugs targeted to multiple viral proteins to minimize the development of resistance. The membrane protein described here, p7, provides a novel target that may function in such a setting.

HCV is an enveloped virus with a positive single strand of RNA genome of approximately 9.6 kb, which is translated into a 3000-amino acid polyprotein that is cleaved by intracellular and viral proteases to yield 10 mature proteins.[5,6] These proteins are divided into two classes, structural and nonstructural (NS) proteins. The structural protein core and envelope glycoproteins, E1 and E2, comprise the virion. Nonstructural proteins NS2, NS3, NS4A, NS4B, NS5A, and NS5B modulate host metabolism and replication of viral RNA. Notably, the nucleotide sequence for a small 63-amino acid hydrophobic transmembrane protein, p7, is located between the sequences that encode the structural and nonstructural proteins.[5]

p7 has previously been shown to be essential for efficient virus particle assembly and release, but not required for RNA replication.[6] p7 is localized to the endoplasmic reticulum. Under the conditions used for electron microscopy, the protein appears to oligomerize as heptamers or hexamers.[7,8] However, sodium dodecyl sulfate gels and narrow nuclear magnetic resonance (NMR) line widths are consistent with the protein being a monomer in micelles. The oligomers may account for the apparent channel activity of p7, which has been demonstrated in phospholipid bilayers.[9,10] Although the role of ion channel activity in the viral life cycle remains uncertain, it can be blocked by a variety of compounds, including amantadine, hexamethylene amiloride (HMA), and a number of iminosugar derivatives, demonstrating the oligomeric form is a potential drug target.[9−13]

The overall structure of p7 consists of two transmembrane (TM) segments, TM1 and TM2, connected by a short, conserved interhelical loop.[14,15] However, the structure is more complex than this. As indicated in Figure 1C, residual dipolar couplings (RDCs) have identified seven distinct structural elements in the protein, including four helical regions that constitute the two transmembrane segments.[16] The first segment (TM1) spans from residue 6 to 3 and the second

Received: May 27, 2013
Revised: July 8, 2013
Published: July 10, 2013

dx.doi.org/10.1021/bi4006623 | *Biochemistry* 2013, 52, 5295−5303

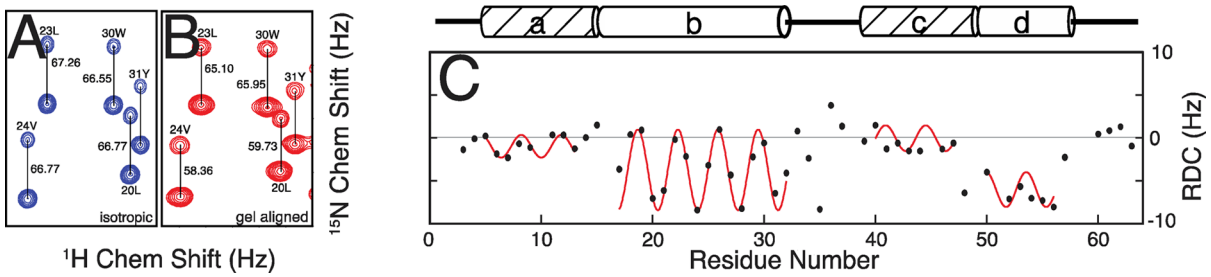

Figure 1. Measurement and analysis of RDCs performed on p7 in 1,2-dihexanoyl-*sn*-glycero-3-phosphocholine and aligned in a polyacrylamide gel. Panels A and B are spectra showing examples of measurements of RDCs using an in-phase/antiphase (IPAP) HSQC experiment on an isotropic sample (A) and a sample that is weakly aligned in a 6% charged and compressed polyacrylamide gel (B). (C) Measured RDCs plotted as a function of residue number. Dipolar waves were fit to the four helical regions shown in the plot (a–d). RDCs for helices a and c are near 0, while those for helices b and d vary drastically, suggesting that the aforementioned are more dynamic.

segment (TM2) from residue 38 to 58. The protein's termini face the lumen of the ER with the interhelical loop region protruding into the cytosol.[14,15] Previous NMR studies have also shown that the helices are tilted ∼10° and ∼25° from the bilayer normal.[17] The magnitudes of the RDCs also revealed the presence of substantial backbone motions in the first and third helical regions of the protein. In particular, tryptophan 48 and proline 49 appear to be highly dynamic. Interestingly, this tryptophan residue is strictly conserved throughout the genotypes of p7.

Recent results suggest that p7 is critical for functions in virus assembly unrelated to its channel activity.[18] Furthermore, p7 may act in unison with HCV proteins E1, E2, and NS2, suggesting that its biological functions and possibly its ion channel activity are regulated by specific protein–protein interactions.[19] A goal of our structural studies is to determine how specific protein–protein interactions, such as those between p7 and NS2, impact channel activity, virion assembly, and the release of viral progeny.

It is important to acknowledge the uncertainties associated with studying membrane proteins in any membrane-mimicking environment other than phospholipid bilayers. However, we have extensive experience with these types of samples[20] and have found that the short chain phospholipid, 1,2-dihexanoyl-*sn*-glycero-3-phosphocholine (DHPC), is generally a good choice as a minimally perturbing detergent for solubilizing p7 for solution NMR spectroscopy. Except for the length of its hydrocarbon chains, its chemical properties are identical to those of the phospholipids that assemble into bilayers; in particular, it has two hydrophobic chains connected to a phosphocholine headgroup.

RDCs are highly reliable sources of structural information for helical membrane proteins because they report on the regular patterns of secondary structure as well as the backbone dynamics of the protein. Moreover, RDCs are important because there are major limitations in measuring "long-range" nuclear Overhauser enhancements (NOEs) among hydrogens in helical membrane proteins in micelles.[21] Tryptophan 48 was investigated not only because of its anomalous location (tryptophan residues are typically located at the interface between headgroups and hydrophobic residues of phospholipids) but also to follow up on some preliminary calculation-based evidence that the dynamics of the third helical region was attenuated by mutating this to a nonaromatic residue. Additionally, other interactions of this residue were investigated. Specifically, the interactions of tryptophan 48 with the proximal tyrosine residues 31, 42, and 45 were examined.

Additional structural characterization of p7 was achieved through the observation of paramagnetic relaxation effects (PREs) from manganese ions in solution. This allowed for the identification of, with some degree of certainty, the residues that are accessible to the aqueous solution. The experiments also provided information about the effect of binding by the channel-blocking compounds amantadine, iminosugar derivative *N*-nonyl-deoxynojirimycin (*N*N-DNJ), and 5-(*N*,*N*-hexamethylene)amiloride (HMA). Previously, Griffin et al. demonstrated that amantadine could block p7 ion channel activity *in vitro*.[11] Steinmann et al. discovered that the effects of amantadine *in vivo* were associated with specific genotypes. They also showed that deoxynojirimycin (DNJ)-containing iminosugars, such as *N*N-DNJ, had inhibitory effects *in vitro*.[3] These effects not only interfered with the entry of HCV into host cells but also significantly inhibited virus assembly and release. Premkumar et al. also demonstrated the ability of HMA to block p7 ion channel activity.[12] By observing the chemical shifts of individual residues, we were able to identify which residues in the protein are involved in binding, possibly contributing to the design of future compounds that exploit these known interactions.

Nonstructural protein 2 (NS2) interacts with several other HCV proteins, including p7.[18,22] The topology of the first TM of NS2 and the location of these interactions were investigated using a combination of isotopically labeled and unlabeled transmembrane domains of both p7 and NS2. This method provides a way of looking at the effect on each of the proteins without complicating the spectra. These experiments provide a starting point for examining the interactions of the full-length versions of both proteins.

EXPERIMENTAL PROCEDURES

Protein Expression and Purification (p7, p7W48A, and NS2 TM1). Samples of p7 from genotype J4 were prepared as previously described.[23] Mutant W48A was prepared using a Quikchange Lightning Site-Directed Mutagenesis Kit (Agilent) and primers synthesized (Allele) to replace the tryptophan at position 48 with alanine. The two primers used were GCTGCTTACGCTTTCTACGGTGTTGCGCCGCTGCTGCTGCTGCTGC and GCAGCAGCAGCAGCAGCGGCGCAACACCGTAGAAAGCGTAAGCAGC. The codons in the mutation site are underlined. The DNA was transformed into XL10 Gold Competent cells (Agilent) and plated on LB agar. The mutation was confirmed by sequence analysis (Eton Biosciences) of individual colonies. The DNA was purified from an overnight LB growth with the cells containing the

dx.doi.org/10.1021/bi4006623 | *Biochemistry* 2013, 52, 5295–5303

correct sequence and transformed into BL21(DE3) (Agilent) cells for protein expression. The protein was expressed and purified the same way as the wild-type protein using nickel affinity chromatography, chemical cleavage from the fusion protein, and reverse-phase high-performance liquid chromatography (HPLC) (Waters).

The same expression vector and purification protocol that were used for p7 were applied to a construct corresponding to the first transmembrane helix of NS2 of HCV. NS2 TM1 was cloned using genotype J4, the same genotype that was used for p7. Oligonucleotides were purchased from Allele to clone the amino acid sequence LDREMAAASSGGAVLVGLVFLTLSPYYK. Forward primer CGGGGAAGCTTATGCTTGACCGTGAAGCTGCTGCTTCTTCTGGTGGTGCTGTTCTGGTTGGTCTGGTTTTCCTGACCCTGTCTCCG and reverse primer CCCCGGATCCTCATCATTTTTTTTTTTTTTTTTTGTAGTACGGAGACAGGGTCAGGAAAACCAGACCAACCAGAACAGCACCACC were elongated to obtain the insert product. The DNA was cut and ligated into the pHLV TrpLE vector using the restriction enzymes *Hin*dIII and *Bam*HI (New England Bioloabs). The insert included a codon for a methionine at the N-terminus of the protein for chemical cleavage and five additional lysines at the C-terminus to assist with the solubility of the protein during purification and sample preparation. Milligram amounts of the labeled polypeptide were prepared for NMR experiments.

Sample Preparation. Samples for solution NMR experiments were prepared as described previously.[23] Briefly, the purified protein, dried following HPLC purification, was dissolved in 400 mM DHPC (Avanti Polar Lipids Inc.) and diluted to an aqueous solution with a final concentration of 125 mM DHPC. D_2O was added to a final concentration of 10% to provide a signal for the spectrometer lock, and the final protein concentration was 0.5 mM. The pH was adjusted to 4.0 for all samples to ensure NMR spectra were well resolved and directly comparable to those analyzed previously.[23] The protein sample was transferred to a standard 5 mm tube for the NMR experiments.

For RDC measurements, the isotropic sample was transferred to a Shigemi (Shigemi Inc.) tube containing a dried 6% neutral polyacrylamide gel that was originally cast in a 3 mm NMR tube and cut to 3 cm in length. The plunger of the NMR tube was set to a length of 2.1 cm to allow the gel to absorb the isotropic protein-containing sample in 125 mM DHPC. The compressed gel resulted in weak alignment of the protein in the NMR sample.

The samples for PRE measurements were prepared by adding chelated manganese to unaligned samples of p7-containing DHPC in aqueous solution. The chelated metal was prepared by adding manganese sulfate to ethylenediaminetetraacetic acid (EDTA) (0.5 M) at pH 8.0 and sufficient time was allowed for a chelated precipitate to form. The precipitate was centrifuged, and the pellet was washed twice with methanol and once with ethanol. The washed complex was dried by lyophilization and a stock solution of 200 mM was prepared in 1 M HEPES [4-(2-hydroxyethyl)-1-piperazineethanesulfonic acid buffer]. The solution was added to the NMR sample at a final Mn^{2+}-EDTA concentration of 10 mM. To make sure that the addition of the buffer did not affect the isotropic signals, a sample with just the buffer added was used as a control.

NMR Experimental Measurements. The NMR experiments were performed on a 600 MHz Bruker spectrometer using a triple-resonance cryoprobe (^1H, ^{13}C, and ^{15}N) with three-axis pulsed gradients. The chemical shift frequencies were referenced to the proton resonance of water set to 4.70 ppm. The experiments were performed at 50 °C. Most of the $^1H-^{15}N$ correlation experiments were performed using the fast-HSQC pulse sequence.[24]Typical experiments involved the acquisition of 1024 t_2 points for 256 t_1 increments.

The backbone amide J couplings were measured using a modified $^1H-^{15}N$ HSQC experiment based on the in-phase/antiphase (IPAP) measurement of JD splitting. The RDCs were measured by taking the difference in JD coupling between an isotropic and a weakly aligned sample of p7-containing DHPC micelles.

The NMR data were processed using NMRPipe,[25] and the figures were prepared using Sparky (T. D. Goddard and D. G. Kneller, *SPARKY 3*, University of California, San Francisco, CA). RDCs were analyzed using Matlab (Mathworks). A sliding window method was used to fit sinusoidal waves with a periodicity of 3.6 residues to the data to predict helical regions, as described previously.[16]

Structure Calculations. A two-stage combined protocol[26,27] was employed to calculate the structure of p7 in DHPC micelles. The determination of the structure is illustrated in Figure 2. In the first stage, 10000 initial structures were generated in CS-Rosetta.[28] Fragment candidates were based on 58 HN, 61 N, and 63 Cα chemical shift frequencies. All of the structures were relaxed under the influence of the NH RDC data using Rosetta. In both steps, the implicit membrane potential flag was on to mimic a membrane-like environment. After relaxation, the 1000 lowest-energy structures were chosen from the most populated cluster, which was calculated from 10000 structures. Forty percent of the 10000 relaxed structures fell into the most populated cluster, while the second most favored cluster contained 22% of the structures. The lowest-energy structure identified in the subset of 1000 selected structures was used as the initial structural model of p7.

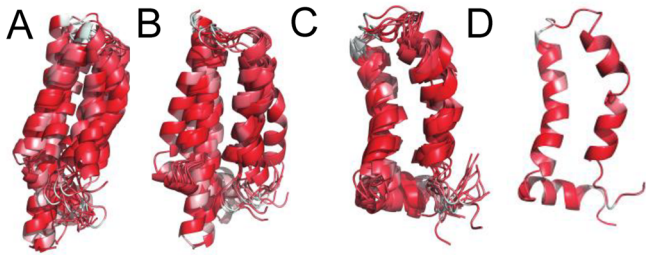

Figure 2. Characterization of the stepwise method for determining the structure of p7 from the measured NMR data. (A) The chemical shifts (Cα, HN, and N) were used as the sole constraint in the CS-Rosetta calculation. The cluster shown consists of the 10 lowest-energy structures from 10000 decoys that were generated. (B) Ten lowest-energy structures of 10000 relaxed initial structures in the presence of residual dipolar couplings as angular constraints. This set of structures converges over a larger portion of the backbone, including an overlay of helix a, which is a result of including orientation information provided by residual dipolar couplings. (C) Ten lowest-energy structures calculated using the Xplor-NIH refinement protocol using the representative structures from the Rosetta calculation. The backbone rmsd for this ensemble is 2.18 Å. Although the rmsd is relatively low for a membrane protein, there is still variation in the mobile region, particularly the start of helix c. (D) A single average structure from the Xplor-NIH refinement cluster was calculated.

dx.doi.org/10.1021/bi4006623 | *Biochemistry* 2013, 52, 5295−5303

Average dihedral angles and their deviations were calculated from the group of 1000 selected low-energy structures for further refinement using Xplor-NIH.

In the second stage, structure refinement was performed using a simulated annealing protocol with Xplor-NIH torsion angle molecular dynamics and the experimental restraints. The temperature was reduced from an initial value of 1000 K to 50 K in steps of 12.5 K. k_{ta} = 200 kcal mol^{-1} rad^{-2}, and k_{rdc} was gradually increased from 2 to 5 kcal mol^{-1} rad^{-2}. The calculation also includes the Xplor-NIH potential for knowledge-based torsion angles with ramped force constants of 0.002−1 kcal mol^{-1} rad^{-2}. k_{vdw} and s_{vdw} were geometrically increased from 0.004 to 4 kcal mol^{-1} Å^{-4} and from 0.9 to 0.8 kcal mol^{-1} Å^{-4}, respectively. A total of 100 structures were calculated, and the 10 lowest-energy structures were accepted for analysis.

Molecular Dynamics Simulations. The 1-palmitoyl-2-oleoylphosphatidylcholine (POPC) bilayer generated and solvated with TIP3P waters in VMD[29] was equilibrated for 1 ns. The lowest-energy structure from the Xplor-NIH refinement was selected. After p7 had been embedded into the *de novo* bilayer, the overlapped water and lipid molecules were removed. This resulted in 80 lipid molecules and 12669 water molecules. A 50 ns simulation was performed after 10000 steps of minimization at 310 K and a constant pressure in NAMD[30] with the CHARMM27 force field.

Drug Binding Studies. Drug binding studies were performed using amantadine (Sigma-Aldrich), hexylmethylamiloride (HMA) (Sigma-Aldrich), and *N*-nonyl-deoxynojirimycin (*N*N-DNJ) (Toronto Chemical Company). Experiments were performed by adding the appropriate compound, either in water or in DMSO, at a concentration that was 20 times greater (10 mM) than that of the protein (0.5 mM). The pH of the sample was measured to ensure that the sample conditions were consistent with those of the control experiment. A ^{1}H−^{15}N HSQC experiment was performed using the same parameters as the control. The chemical shifts of the protein resonances were measured. Difference plots were made that utilized both ^{1}H and ^{15}N shifts using the term $[(\Delta\delta H)^2 + (\Delta\delta N/5)^2]^{1/2}$.

RESULTS

Chemical Shifts and Residual Dipolar Couplings. The amide proton and nitrogen shifts were measured from the two-dimensional ^{1}H−^{15}N HSQC spectra, while the α-carbon chemical shifts were measured from the three-dimensional HNCA spectra that were used to assign the protein resonances. In this experiment, the magnetization is transferred from the amide proton to the amide nitrogen, and then to the α-carbons of the same residue and the preceding residue. The magnetization pathway provides the chemical shifts of the carbon nuclei and assigns the backbone resonances. The dispersion of resonances in the HSQC spectra demonstrated that the protein is folded in the DHPC micelles, and a plot of the Cα chemical shifts as a function of residue number gives a preliminary indication of the secondary structure being composed of mostly α-helices based on the upfield chemical shifts from random coil values.

As described in Experimental Procedures and in previous publications, p7 could be weakly aligned in a compressed polyacrylamide gel for RDC measurements.[31] The residual dipolar couplings were measured for all of the backbone amide sites using an IPAP ^{1}H−^{15}N HSQC experiment on an isotropic sample and a weakly aligned gel sample (Figure 1A,B). The differences in the measured splittings, which ranged from 4 to −8 Hz, were plotted as a function of residue number (Figure 1C). This was possible because all of the resonances have been assigned to specific backbone sites in the protein.[16] Sinusoidal waves were fit to the data using a periodicity of 3.6 residues per turn, appropriate for an α-helix, to identify those residues in helical regions of the protein.[32] Four separate waves resulted from the fitting procedure, as shown in Figure 1C. The amplitudes of the waves suggest that the helical segments labeled a and c have internal motions caused by generally low values of residual dipolar couplings. Helices b and d appear to be fully structured on the NMR timescales. This result is in general agreement with the previous analysis of the secondary structure of p7.[31]

Structure Calculations. For the structure calculations of p7, the chemical shift-associated molecular fragment replacement (MFR) method was used to obtain a starting structure that could be refined using RDC data as constraints. The initial set of structures calculated from Rosetta (Figure 2A) utilized the primary sequence of p7. The set shows convergence of the polypeptide backbone structure. An interesting feature, confirmed by the structure calculations, is that W48, a residue that is normally at the interface of the polar headgroups and the hydrophobic side chains of the lipids, is buried within the lipid bilayer in p7. When the RDC data were added as constraints to the calculation, the largest change was observed in the orientation of helical segment a (Figure 2B). Consequently, the relative orientation of the two transmembrane segments changed. The refinement of these structures in Xplor-NIH using the same constraints caused the structures to converge with an rmsd of the backbone atoms of 2.18 Å (Figure 2C). An average structure from the cluster of the 10 lowest-energy structures was calculated (Figure 2D).

The average structure is shown in Figure 3 from three different perspectives. From these views, the orientation of the four helices can be seen. Helix a has an orientation different from that of helix b and resides almost perpendicular to the membrane-spanning segments. Helices c and d are clearly separated by several residues that include Trp48 and Pro49.

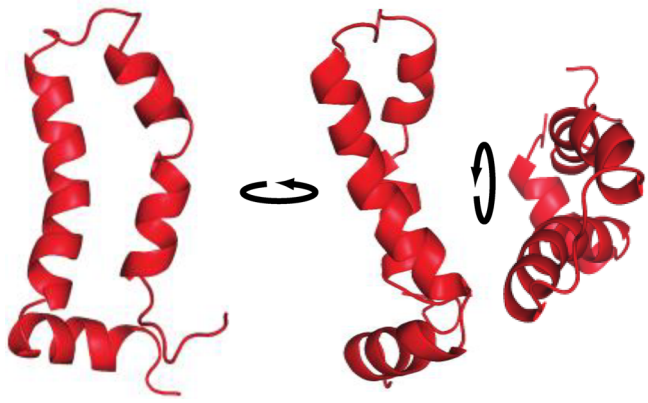

Figure 3. Average calculated structure of p7 from the Xplor-NIH refinement. The structure is the average structure from the lowest-energy cluster. The three views show the orientation of the four helices.

Manganese Data Compared with the Structure. The PRE data[16] were plotted in the form of measured peak intensity as a function of residue number (Figure 4A). Resonance intensities that were reduced by at least 50% are highlighted on the structure of p7 (Figure 4B). The residues that are exposed to the aqueous solvent are strongly affected by the addition of

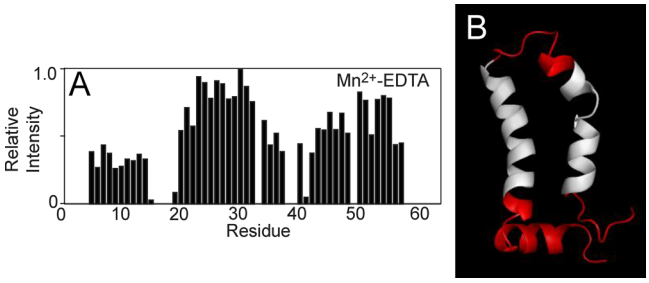

Figure 4. Paramagnetic relaxation effect of manganese on p7 characterized using differential signal intensities measured from $^{1}H-^{15}N$ HSQC spectra. (A) Spectra of p7 measured before and after the addition of Mn^{2+}-EDTA. The relative intensity, or the ratio of the intensities, is plotted vs residue number. The signals with significantly reduced intensities indicate that the associated residues are solvent-exposed. (B) Residues with a >50% reduction in signal intensity are colored red. From this representation, it is obvious which regions of the protein are buried within the hydrophobic region of the DHPC micelle.

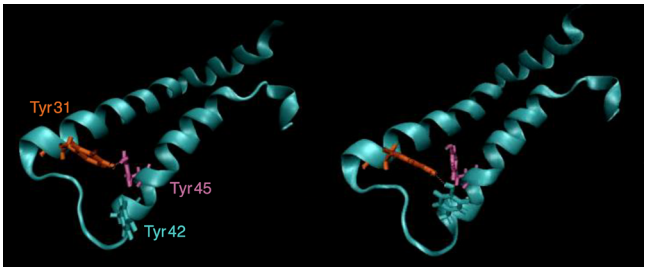

Figure 5. Simulations show evidence of side chain interactions of p7 in an implicit POPC bilayer. Two "snapshots" were taken from a 50 ns MD simulation. The figure shows the hydrogen bonding that takes place between the side chains of tyrosine residues at the interface of the transmembrane segments, Y31 from TM1 and Y42 and Y45 from TM2. The structure on the left shows hydrogen bonding between Y31 and Y45, and the structure on the right shows that hydrogen bonding has switched from Y31 to Y42.

the EDTA-chelated paramagnetic metal. The intensities of the region between the first and second helical segments, a and b (residues 15−18), are reduced, suggesting that these residues are accessible to the chelated manganese in solution. This also suggests that the first helical segment is somewhat shielded from the effects of the chelated manganese within the polar headgroups of the lipids. As illustrated in Figure 4, the loop region (residues 28−36) and the C-termini (residues 58−63) are also exposed to the aqueous solution.

Simulations. To examine the dynamics of p7 in a lipid environment, the refined structure of p7 was placed in a *de novo* membrane made of POPC and allowed to relax over a period of 50 ns. Because of the chain length difference of the lipids used for NMR experiments (six carbons) and the simulations (16 and 18 carbons), some differences in the overall structure are anticipated. These differences do not necessarily affect the dynamics or intramolecular interactions that take place within the protein. The simulations are intended to provide confirmation of the experimental findings described here and to set the stage for a more detailed study of these characteristics of the protein in phospholipid environments. During the simulation, several side chain interactions were observed. The most interesting of these were among tyrosine residues near the interhelical loop, as illustrated in Figure 5. Simulations suggest that hydrogen bonding between tyrosine 31 of the first transmembrane helix and tyrosines 42 and 45 of the second transmembrane helix occurs. During the simulation, a switch of the bond from one tyrosine to the other was observed. This specific switch may be associated with the intramolecular motions observed in helical segment c.

Drug Binding. Several known channel-blocking compounds have been shown to alter the ion channel activity of p7. These commercially available compounds were added directly to the NMR samples. As shown in Figure 6, when the ^{1}H and ^{15}N chemical shift changes are plotted as a function of residue number, there is evidence of site-specific interactions between the drugs and residues on the protein. It is apparent that the three compounds, amantadine, *N*N-DNJ, and HMA, interact with the protein differently. Amantadine and *N*N-DNJ have a stronger effect on the chemical shifts of the terminal regions, while HMA alters the chemical shifts of residues in the loop region. Caution is required in this interpretation because of differences in their hydrophobicity and hence access to the residues in the protein that are within the hydrocarbon core of the micelles.

NS2 TM1 Expression and Purification. NS2 and p7 have been shown to co-localize in the ER membrane, are believed to be involved in virus assembly,[18] and may interact with each other within the membrane. To determine possible interactions between the two proteins, the NS2 construct derived from the same genotype, J4, as p7 was expressed and purified. To simplify the identification of involved residues and accelerate the research, a construct corresponding to the first TM of NS2, thought to be the crucial segment for these interactions, was used.[33] NS2 TM1 was successfully expressed as a fusion protein, identical to the p7 construct, and was directed to the inclusion bodies of the cells. Using a purification protocol similar to that used for p7, the inclusion bodies were isolated during lysis, cleaved, and purified via HPLC. Milligram amounts of isotopically ^{15}N-labeled protein that could be incorporated into DHPC micelles were obtained. These samples appeared to be well behaved under the same conditions employed for the p7 samples.

The resonances in the two-dimensional HSQC spectrum of the NS2 construct (Figure 7A) are well dispersed, and 85% of the backbone signals were assigned using a single two-dimensional $^{1}H-^{15}N$ HSQC NOESY experiment. HSQC spectra of the transmembrane domain of NS2 in DHPC micelles were measured before and after the addition of unlabeled p7 to the sample. Several of the NS2 resonances were obviously shifted in the spectra, indicating that p7 was interacting with specific residues (Figure 7B,C). A plot of the chemical shift changes as a function of residue number upon the addition of p7 shows that the residues affected the most are those that are at the center of the transmembrane helix, indicating that these interactions are taking place within the membrane (Figure 7D). Ala12 and Val15, the two residues that are most affected, are three residues apart, which is consistent with their residing on the same face of the helix.

The effect of addition of the NS2 construct on p7 spectra was also measured. When the unlabeled NS2 construct was added to a sample of uniformly ^{15}N-labeled p7 protein, spectral changes were observed. Interestingly, the residue that displays the largest change in chemical shift frequencies is Trp48. This residue is also predicted to be in the center of the membrane, as discussed above.

DISCUSSION

The schematic drawing of p7 and NS2 in the top of Figure 8 shows antiparallel orientations of the transmembrane segments

dx.doi.org/10.1021/bi4006623 | *Biochemistry* 2013, 52, 5295−5303

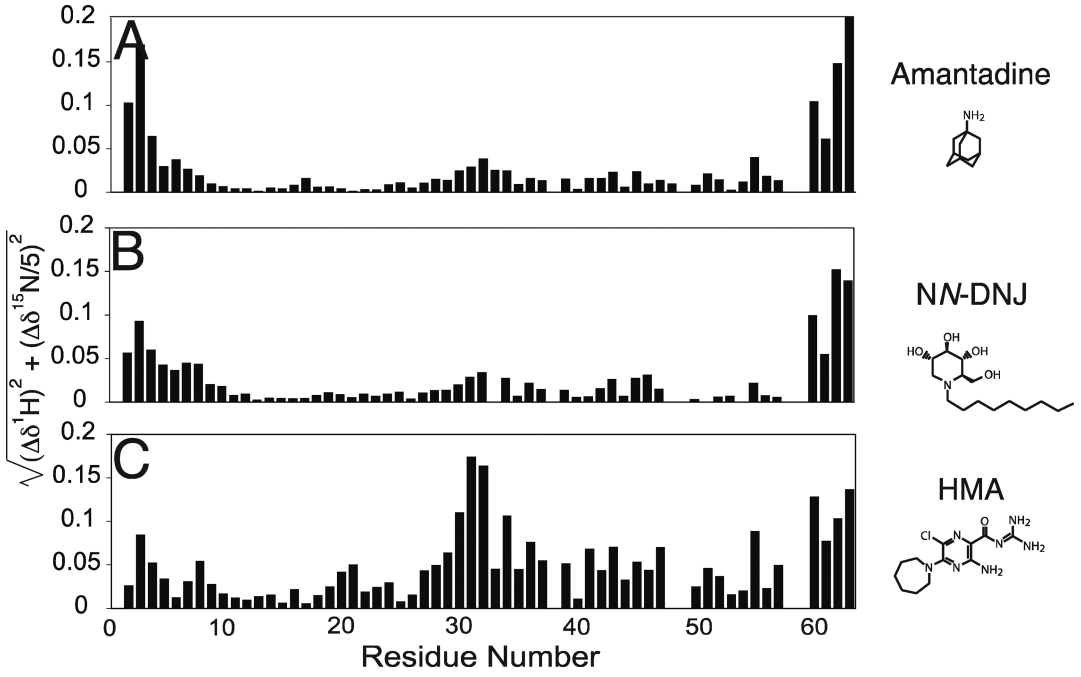

Figure 6. Chemical shift differences plotted as a function of residue number show the changes induced when different channel-blocking compounds are added to the NMR sample of p7. The chemical shifts of the backbone amide proton and nitrogen are taken into account and plotted vs the primary sequence. (A) Amantadine and the iminosugar derivative. (B) *N*N-DNJ appears to interact at the terminal regions, while (C) hexylmethylamiloride has a stronger effect on the loop region. These three plots show how compounds interact with p7 in different regions of the protein.

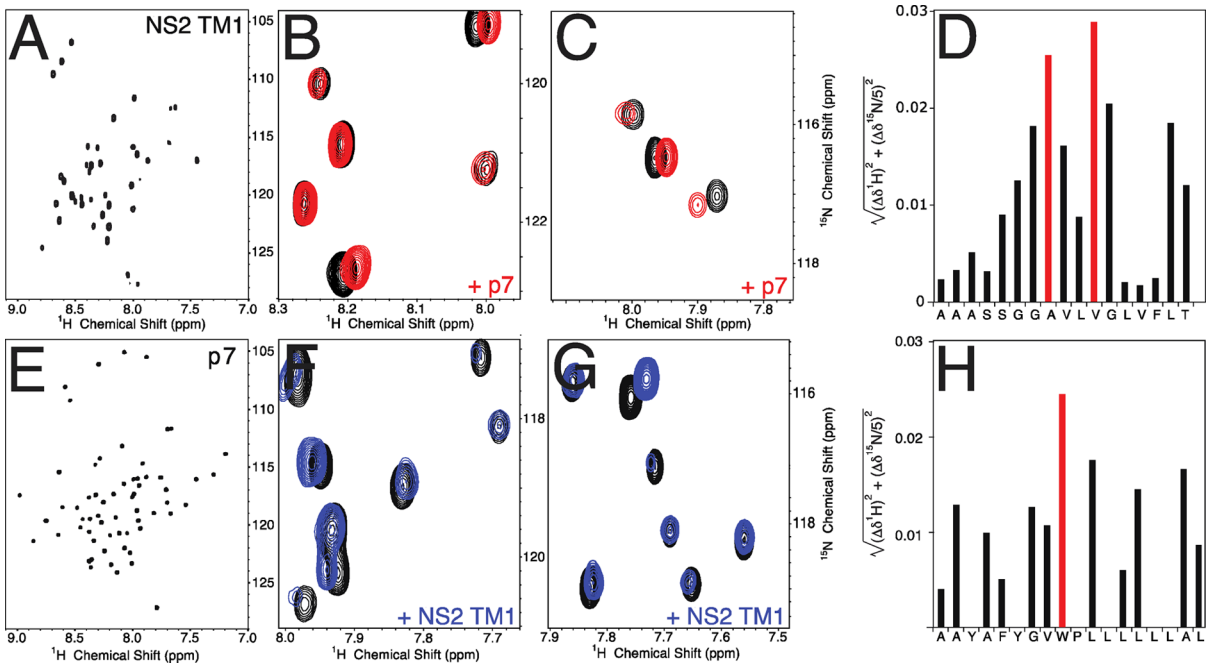

Figure 7. Protein−protein interactions between J4 p7 and NS2 TM1 in DHPC measured using chemical shift changes. (A and E) Baseline $^{1}H-^{15}N$ HSQC spectra of NS2 TM1 and p7, respectively. (B and C) Regions from the NS2 TM1 HSQC spectra measured after the addition of unlabeled p7 (red) to labeled NS2 (black) shown to highlight some of the chemical shift perturbations to the NS2 TM1 protein. (F and G) Similar portions of the p7 HSQC spectra measured after the addition of unlabeled NS2 (blue) to labeled p7 (black). The proteins were added at a 1:1 concentration ratio. These spectra clearly show chemical shift changes indicating structural perturbations and interactions in both proteins. (D and H) Plot of the chemical shift changes as a function of residue showing that the interactions are likely taking place within the transmembrane regions of both proteins.

within the bilayer. The sequence alignment of the two proteins (Figure 8, bottom) shows that the Trp48 residue of p7 and Ala12 and Val15 of NS2 are aligned near the center of the membrane when boundaries of the transmembrane helices are aligned. Because significant chemical shift changes were limited to one residue of p7 and two residues of NS2, the helices are likely to have different tilt angles within the bilayer. The tilt of the second transmembrane helix of p7 was previously found to

dx.doi.org/10.1021/bi4006623 | *Biochemistry* 2013, 52, 5295−5303

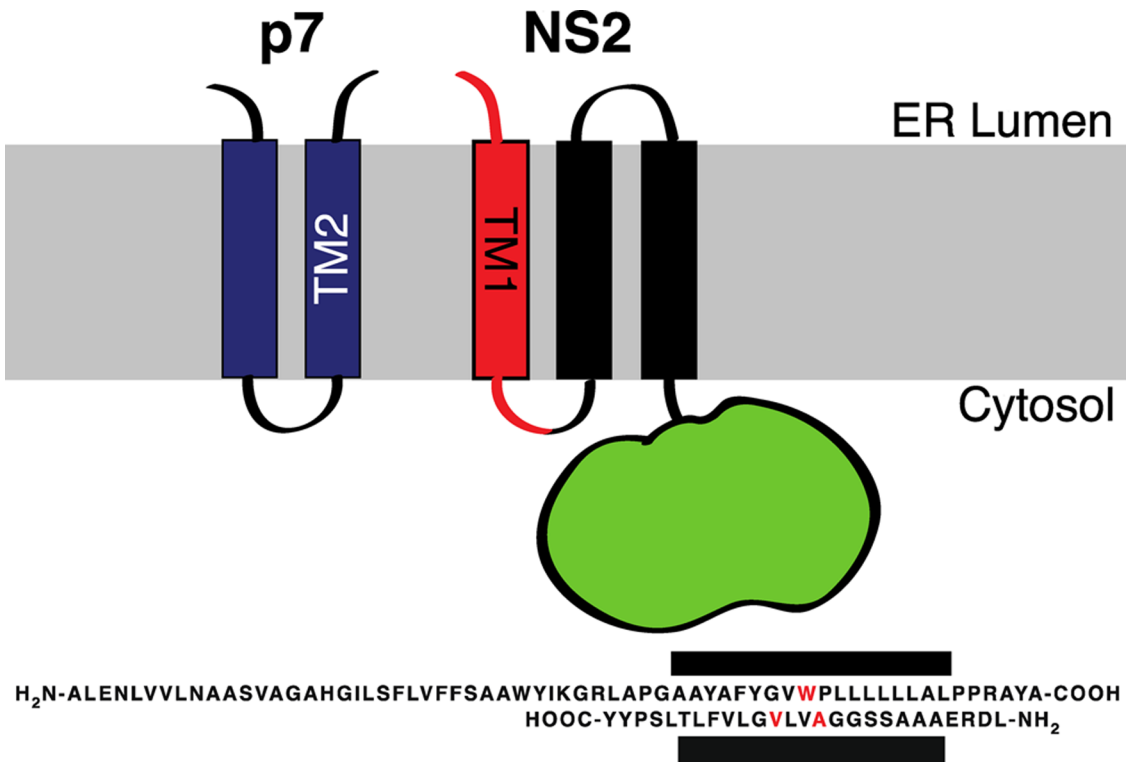

Figure 8. Cartoon illustration representing p7 and NS2 in the membrane of the endoplasmic reticulum. The antiparallel arrangement of TM2 of p7 and TM1 of NS2 is shown in the diagram. Below the diagram is an alignment of the respective p7 and NS2 TM1 sequences with a black rectangle corresponding to the TM regions of the proteins. The residues that have the largest chemical shift changes in Figure 6 are colored red in the sequence.

be approximately 10° relative to the bilayer normal in a DMPC bilayer.

Along with the protein−protein interactions, drug−protein interactions were examined using several compounds with p7. Unlike the NS2 studies, in which both components were incorporated into the lipid environment, the drug compounds were added to the solution. This limited the observable interactions to the loops and terminal regions of the protein because the drugs, with the exception of amantadine, are not hydrophobic. Although specific amino acids could be identified as interacting with the drugs, the results highlight the need for performing these studies in a bilayer environment where the protein can form the oligomers that have been observed in cryo-electron microscopy studies.

The simulation studies presented here provide an initial attempt to understand the reason p7 is so dynamic. The switching of the hydrogen bond at the tyrosine side chains during the simulations is an interesting finding that requires close analysis of other residues at the interface of the transmembrane segments. It is clear that the mobile section of TM2 ends at the position of Trp48 and Pro49. The tryptophan appears to result in steric hindrance that maintains a separation of the two segments. To examine this hypothesis, we created a point mutation in p7 at the tryptophan residue. The mutant protein, p7 W48A, was successfully expressed and purified. The HSQC spectrum of the mutant protein (Figure 9A) indicates that it is well behaved under the same sample conditions that were used for the wild-type protein. All of the signals could be assigned by comparison with the spectra of the wild-type protein. A plot of the chemical shift changes as a function of residue number indicates that the structural changes to the backbone are not limited to TM2 in the region where the mutation was made (Figure 9B). Although the changes appear to be localized to several short regions of the protein, suggesting that the global structure of p7 remains the same, one of these regions is in the middle of TM1. The residues most affected are phenylalanines 22, 25, and 26. This indicates the mutation has an interhelical effect. A plot of the relative intensity indicates that the third helical region is less dynamic as a result of the residue change, which may suggest that the placement of a less bulky alanine at site 48 allows the two helices of the protein to move closer together, leading to a possible stacking of the tyrosine rings and a more stable structure. Another region where the chemical shifts have changed is between the loop and helix c. This might indicate that this is a hinge point that is responsible for accommodating the movement of TM2 to a position that is closer to TM1.

p7 is a remarkably complex protein considering that it has only 63 residues and its secondary structure is dominated by two hydrophobic transmembrane helices. Another NMR study of p7 in DPC micelles in solution suggests that it exists as a hexamer, and the resulting channel is more likely to be a dominant mechanism of biological activity.[8] In contrast, the structural and dynamic features identified with our NMR experiments on monomers of p7 in DHPC micelles in solution indicate that its biological roles may be more numerous and multifaceted than simply acting as a channel. Indeed, its channel activity may be secondary to its principal biological activities, a notion reinforced by the position of its gene between those for the nonstructural and structural proteins of HCV. At least some of its functions are likely to involve interactions with other proteins, such as those shown in the example of p7 interacting with NS2 in Figure 8. Protein−protein interactions, as well as possible channel functions, are likely to be affected by its structure and changes in its in

dx.doi.org/10.1021/bi4006623 | *Biochemistry* 2013, 52, 5295−5303

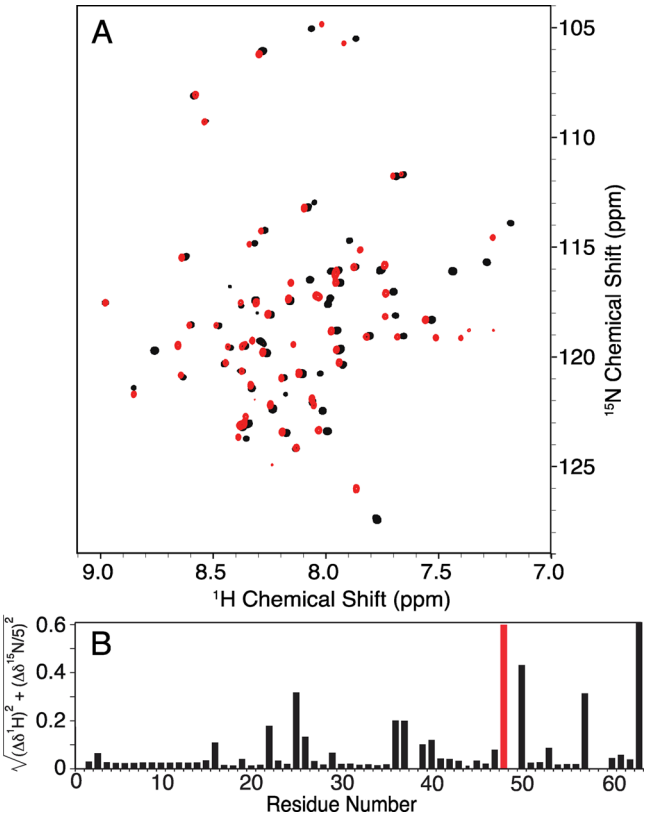

Figure 9. Overlay of HSQC spectra of wild-type p7 (black) and mutant p7 W48A (red) showing chemical shift differences. (A) The HSQC spectra of wild-type p7 and p7 W48A were recorded at 600 MHz, 50 °C, and pH 4.0 in 125 mM DHPC micelles (Experimental Procedures). (B) Chemical shift changes are clearly evident in the second TM region where the mutation was made. Several residues directly across from residue 48 also show a degree of shift change, including three phenylalanine residues (Phe22, Phe25, and Phe26).

response to the life cycle of the virus and the addition of drugs.

AUTHOR INFORMATION

Corresponding Author

*Department of Chemistry, University of California at San Diego, La Jolla, CA 92093. E-mail: sopella@ucsd.edu. Telephone: (858) 822-4820.

Funding

The research was supported by Grants RO1GM066978, R21GM075917, and P41EB002031 from the National Institutes of Health.

Notes

The authors declare no competing financial interest.

ACKNOWLEDGMENTS

We thank Chris Grant and Albert Wu for assistance with instrumentation. We utilized the Biomedical Technology Resource for NMR Molecular Imaging of Proteins at the University of California at San Diego.

ABBREVIATIONS

HCV, hepatitis C virus; NS, nonstructural protein; HMA, 5-(*N*,*N*-hexamethylene)amiloride; *N*N-DNJ, *N*-nonyl-deoxynojirimycin; RDC, residual dipolar coupling; TM1, transmembrane 1; TM2, transmembrane 2; E1, envelope protein 1; E2, envelope protein 2; NOE, nuclear Overhauser effect; DHPC, 1,2-dihexanoyl-*sn*-glycero-3-phosphocholine; PRE, paramagnetic relaxation enhancement; D_2O, deuterium oxide; EDTA, ethylenediaminetetraacetic acid; IPAP, in-phase/antiphase; HSQC, heteronuclear single-quantum coherence spectroscopy; POPC, 1-palmitoyl-2-oleoylphosphatidylcholine; rmsd, root-mean-square deviation.

REFERENCES

(1) Robertson, B., Myers, G., Howard, C., Brettin, T., Bukh, J., Gaschen, B., Gojobori, T., Maertens, G., Mizokami, M., Nainan, O., Netesov, S., Nishioka, K., Shin, I.-T., Simmonds, P., Smith, D., Stuyver, L., and Weiner, A. (1998) Classification, nomenclature, and database development for hepatitis C virus (HCV) and related viruses: Proposals for standardization. International Committee on Virus Taxonomy. *Arch. Virol. 143*, 2493−2503.

(2) Chemello, L., Cavalletto, L., Noventa, F., Bonetti, P., Casarin, C., Bernardinello, E., Pontisso, P., Donada, C., Casarin, P., Belussi, F., et al. (1995) Predictors of sustained response, relapse and no response in patients with chronic hepatitis C treated with interferon-α. *Journal of Viral Hepatitis 2*, 91−96.

(3) Steinmann, E., Whitfield, T., Kallis, S., Dwek, R. A., Zitzmann, N., Pietschmann, T., and Bartenschlager, R. (2007) Antiviral effects of amantadine and iminosugar derivatives against hepatitis C virus. *Hepatology 46*, 330−338.

(4) Tomei, L., Altamura, S., Paonessa, G., De Francesco, R., and Migliaccio, G. (2005) HCV antiviral resistance: The impact of in vitro studies on the development of antiviral agents targeting the viral NS5B polymerase. *Antiviral Chem. Chemother. 16*, 225−245.

(5) Major, M. E., and Feinstone, S. M. (1997) The molecular virology of hepatitis C. *Hepatology 25*, 1527−1538.

(6) Sakai, A., Claire, M. S., Faulk, K., Govindarajan, S., Emerson, S. U., Purcell, R. H., and Bukh, J. (2003) The p7 polypeptide of hepatitis C virus is critical for infectivity and contains functionally important genotype-specific sequences. *Proc. Natl. Acad. Sci. U.S.A. 100*, 11646−11651.

(7) Luik, P., Chew, C., Aittoniemi, J., Chang, J., Wentworth, P., Jr., Dwek, R. A., Biggin, P. C., Venien-Bryan, C., and Zitzmann, N. (2009) The 3-dimensional structure of a hepatitis C virus p7 ion channel by electron microscopy. *Proc. Natl. Acad. Sci. U.S.A. 106*, 12712−12716.

(8) OuYang, B., Xie, S., Berardi, M. J., Zhao, X., Dev, J., Yu, W., Sun, B., and Chou, J. J. (2013) Unusual architecture of the p7 channel from hepatitis C virus. *Nature 498*, 521−525.

(9) Clarke, D., Griffin, S., Beales, L., Gelais, C. S., Burgess, S., Harris, M., and Rowlands, D. (2006) Evidence for the formation of a heptameric ion channel complex by the hepatitis C virus p7 protein in vitro. *J. Biol. Chem. 281*, 37057−37068.

(10) Pavlovic, D., Neville, D. C., Argaud, O., Blumberg, B., Dwek, R. A., Fischer, W. B., and Zitzmann, N. (2003) The hepatitis C virus p7 protein forms an ion channel that is inhibited by long-alkyl-chain iminosugar derivatives. *Proc. Natl. Acad. Sci. U.S.A. 100*, 6104−6108.

(11) Griffin, S. D., Beales, L. P., Clarke, D. S., Worsfold, O., Evans, S. D., Jaeger, J., Harris, M. P., and Rowlands, D. J. (2003) The p7 protein of hepatitis C virus forms an ion channel that is blocked by the antiviral drug, amantadine. *FEBS Lett. 535*, 34−38.

(12) Premkumar, A., Wilson, L., Ewart, G. D., and Gage, P. W. (2004) Cation-selective ion channels formed by p7 of hepatitis C virus are blocked by hexamethylene amiloride. *FEBS Lett. 557*, 99−103.

(13) Steinmann, E., Penin, F., Kallis, S., Patel, A. H., Bartenschlager, R., and Pietschmann, T. (2007) Hepatitis C virus p7 protein is crucial for assembly and release of infectious virions. *PLoS Pathog. 3*, e103.

(14) Carrere-Kremer, S., Montpellier-Pala, C., Cocquerel, L., Wychowski, C., Penin, F., and Dubuisson, J. (2002) Subcellular localization and topology of the p7 polypeptide of hepatitis C virus. *J. Virol. 76*, 3720−3730.

(15) Patargias, G., Zitzmann, N., Dwek, R., and Fischer, W. B. (2006) Protein-protein interactions: Modeling the hepatitis C virus ion channel p7. *J. Med. Chem. 49*, 648−655.
(16) Cook, G. A., and Opella, S. J. (2011) Secondary structure, dynamics, and architecture of the p7 membrane protein from hepatitis C virus by NMR spectroscopy. *Biochim. Biophys. Acta 1808*, 1448−1453.
(17) Cook, G. A., and Opella, S. J. (2010) NMR studies of p7 protein from hepatitis C virus. *Eur. Biophys. J. 39*, 1097−1104.
(18) Popescu, C. I., Callens, N., Trinel, D., Roingeard, P., Moradpour, D., Descamps, V., Duverlie, G., Penin, F., Heliot, L., Rouille, Y., and Dubuisson, J. (2011) NS2 protein of hepatitis C virus interacts with structural and non-structural proteins towards virus assembly. *PLoS Pathog. 7*, e1001278.
(19) Chandler, D. E., Penin, F., Schulten, K., and Chipot, C. (2012) The p7 protein of hepatitis C virus forms structurally plastic, minimalist ion channels. *PLoS Comput. Biol. 8*, e1002702.
(20) De Angelis, A. A., and Opella, S. J. (2007) Bicelle samples for solid-state NMR of membrane proteins. *Nat. Protoc. 2*, 2332−2338.
(21) Tjandra, N., and Bax, A. (1997) Direct measurement of distances and angles in biomolecules by NMR in a dilute liquid crystalline medium. *Science 278*, 1111−1114.
(22) Vieyres, G., Brohm, C., Friesland, M., Gentzsch, J., Wolk, B., Roingeard, P., Steinmann, E., and Pietschmann, T. (2013) Subcellular localization and function of an epitope-tagged p7 viroporin in hepatitis C virus-producing cells. *J. Virol. 87*, 1664−1678.
(23) Cook, G. A., Stefer, S., and Opella, S. J. (2011) Expression and purification of the membrane protein p7 from hepatitis C virus. *Biopolymers 96*, 32−40.
(24) Mori, S., Abeygunawardana, C., Johnson, M. O., and van Zijl, P. C. (1995) Improved sensitivity of HSQC spectra of exchanging protons at short interscan delays using a new fast HSQC (FHSQC) detection scheme that avoids water saturation. *J. Magn. Reson., Ser. B 108*, 94−98.
(25) Delaglio, F., Grzesiek, S., Vuister, G. W., Zhu, G., Pfeifer, J., and Bax, A. (1995) NMRPipe: A multidimensional spectral processing system based on UNIX pipes. *J. Biomol. NMR 6*, 277−293.
(26) Das, B. B., Nothnagel, H. J., Lu, G. J., Son, W. S., Tian, Y., Marassi, F. M., and Opella, S. J. (2012) Structure determination of a membrane protein in proteoliposomes. *J. Am. Chem. Soc. 134*, 2047−2056.
(27) Park, S. H., Das, B. B., Casagrande, F., Tian, Y., Nothnagel, H. J., Chu, M., Kiefer, H., Maier, K., De Angelis, A. A., Marassi, F. M., and Opella, S. J. (2012) Structure of the chemokine receptor CXCR1 in phospholipid bilayers. *Nature 491*, 779−783.
(28) Shen, Y., Lange, O., Delaglio, F., Rossi, P., Aramini, J. M., Liu, G., Eletsky, A., Wu, Y., Singarapu, K. K., Lemak, A., Ignatchenko, A., Arrowsmith, C. H., Szyperski, T., Montelione, G. T., Baker, D., and Bax, A. (2008) Consistent blind protein structure generation from NMR chemical shift data. *Proc. Natl. Acad. Sci. U.S.A. 105*, 4685−4690.
(29) Humphrey, W., Dalke, A., and Schulten, K. (1996) VMD: Visual molecular dynamics. *J. Mol. Graphics 14*, 27−38.
(30) Phillips, J. C., Braun, R., Wang, W., Gumbart, J., Tajkhorshid, E., Villa, E., Chipot, C., Skeel, R. D., Kale, L., and Schulten, K. (2005) Scalable molecular dynamics with NAMD. *J. Comput. Chem. 26*, 1781−1802.
(31) Cook, G., and Opella, S. J. (2010) Secondary structure, dynamics, and architectue of the p7 membrane protein of hepatitis C virus by NMR spectroscopy. *Biochim. Biophys. Acta 1808*, 1448−1453.
(32) Mesleh, M. F., and Opella, S. J. (2003) Dipolar Waves as NMR maps of helices in proteins. *J. Magn. Reson. 163*, 288−299.
(33) Gouklani, H., Beyer, C., Drummer, H., Gowans, E. J., Netter, H. J., and Haqshenas, G. (2013) Identification of specific regions in hepatitis C virus core, NS2 and NS5A that genetically interact with p7 and co-ordinate infectious virus production. *Journal of Viral Hepatitis 20*, e66−e71.